Supporting Information

Multifunctional SnSe-C composite modified 3D scaffolds to regulate lithium nucleation and fast transport for dendrite-free lithium metal anode

Xiaojie Shen, [a] Guangyu Zhao, *[b] and Naiqing Zhang *[ab]

a. State Key Laboratory of Urban Water Resource and Environment, School of Chemistry and Chemical Engineering, Harbin Institute of Technology, China.

b. Academy of Fundamental and Interdisciplinary Sciences, Harbin Institute of Technology, Harbin, 150001, China. Email: zhaogy810525@gmail.com; znqmww@163.com

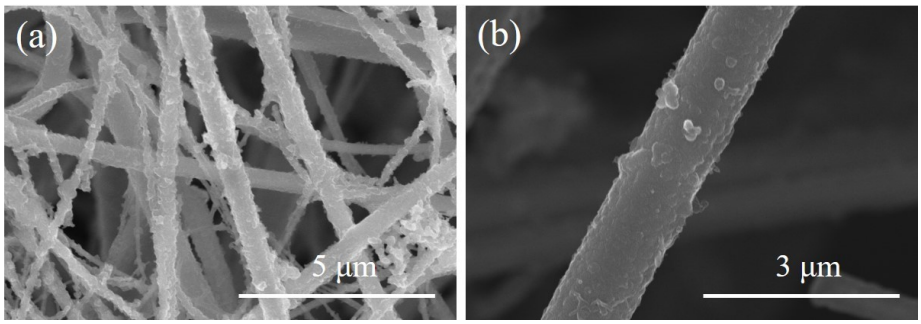

Figure S1. Morphologies of PAni/GFs fabricated by aniline chemical oxidation polymerization on GFs (a) low and (b) high magnification.

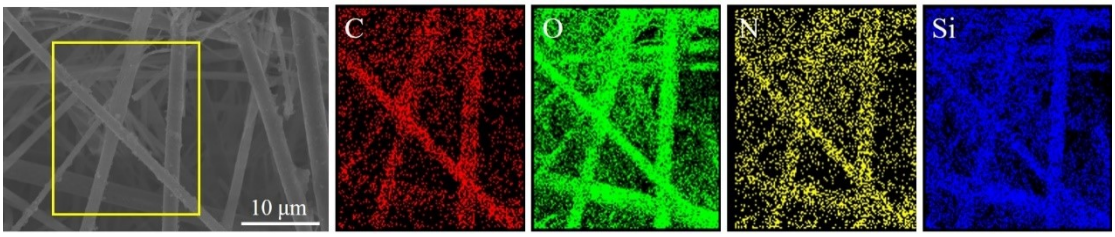

Figure S2. EDS elemental mapping diagram of C, O, N and Si of the PAni/GFs matrix.

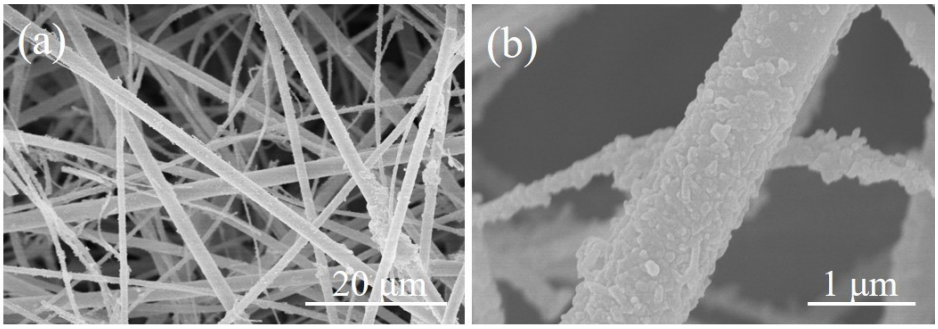

Figure S3. Morphologies of Sn-MOFs/PAni/GFs (a) low and (b) high magnification.

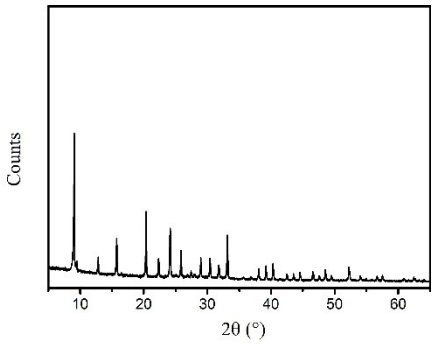

Figure S4. XRD pattern of synthesized of Sn-MOFs.

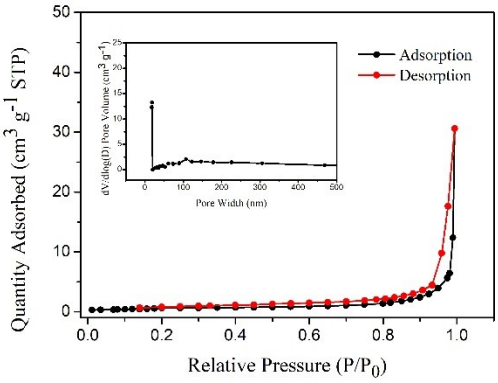

Figure S5. The nitrogen adsorption-desorption isotherm of the Sn-MOFs powder and the inset is corresponding pore-size distribution.

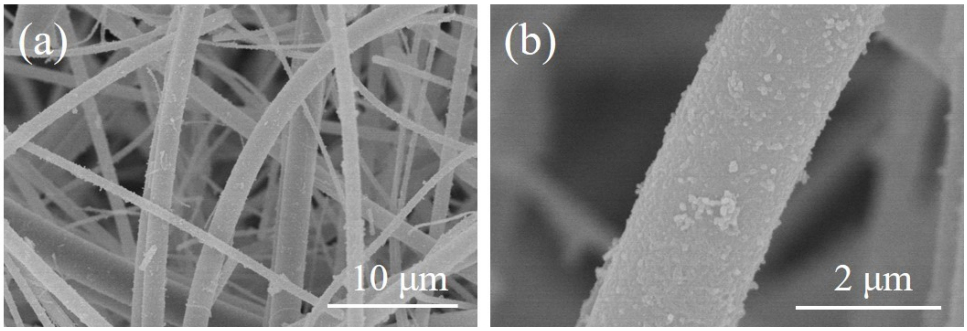

Figure S6. Morphologies of SnO_x-C/MGFs (a) low and (b) high magnification.

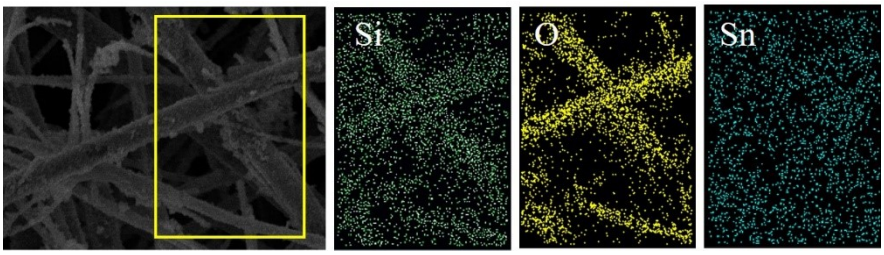

Figure S7. EDS elemental mapping diagram of Si, O and Sn of the SnO_x-C/MGFs matrix.

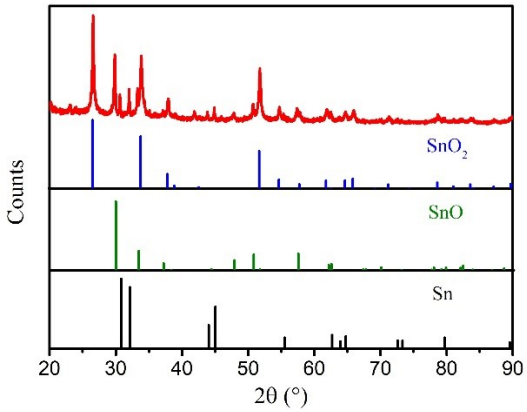

Figure S8. XRD pattern of synthesized of SnO_x-C/MGFs.

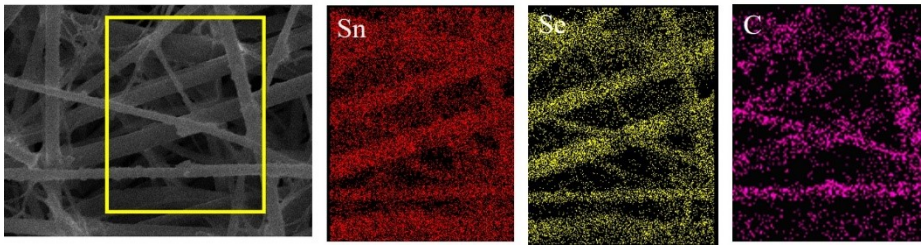

Figure S9. EDS elemental mapping diagram of Sn, Se and C of the SnSe-C/MGFs matrix.

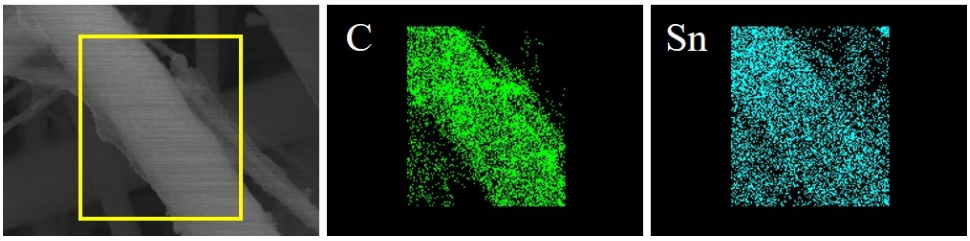

Figure S10. EDS elemental mapping diagram of C and Sn of the Sn-C/MGFs matrix.

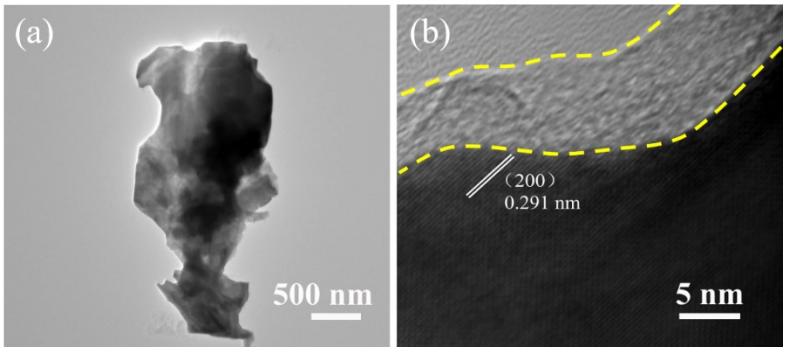

Figure S11. TEM of Sn-C/MGFs: (a) low resolution and (b) high resolution.

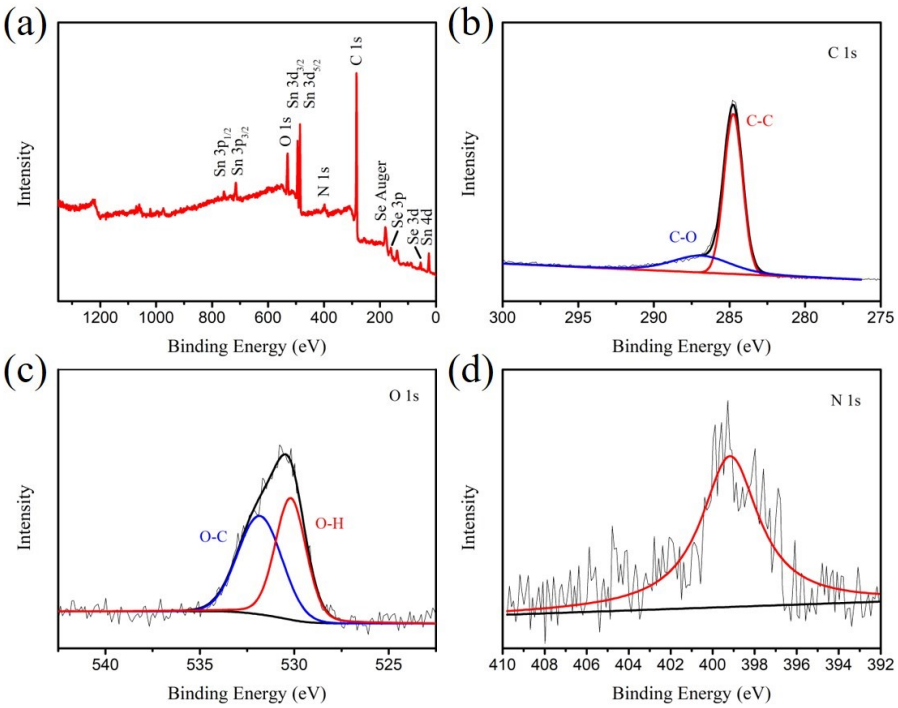

Figure S12. (a) the survey of the SnSe-C/MGFs scaffold XPS spectrum. (b) High-resolution C 1s XPS spectrum. (c) High-resolution O 1s XPS spectrum. (d) High-resolution N 1s XPS spectrum.

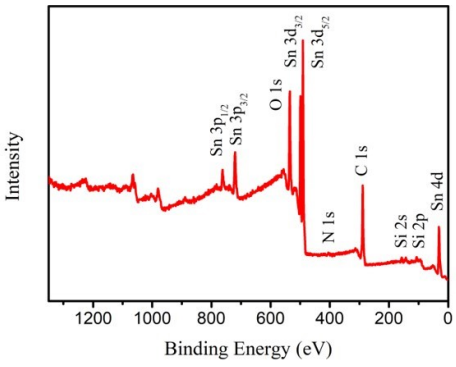

Figure S13. the survey of the Sn-C/MGFs scaffold XPS spectrum.

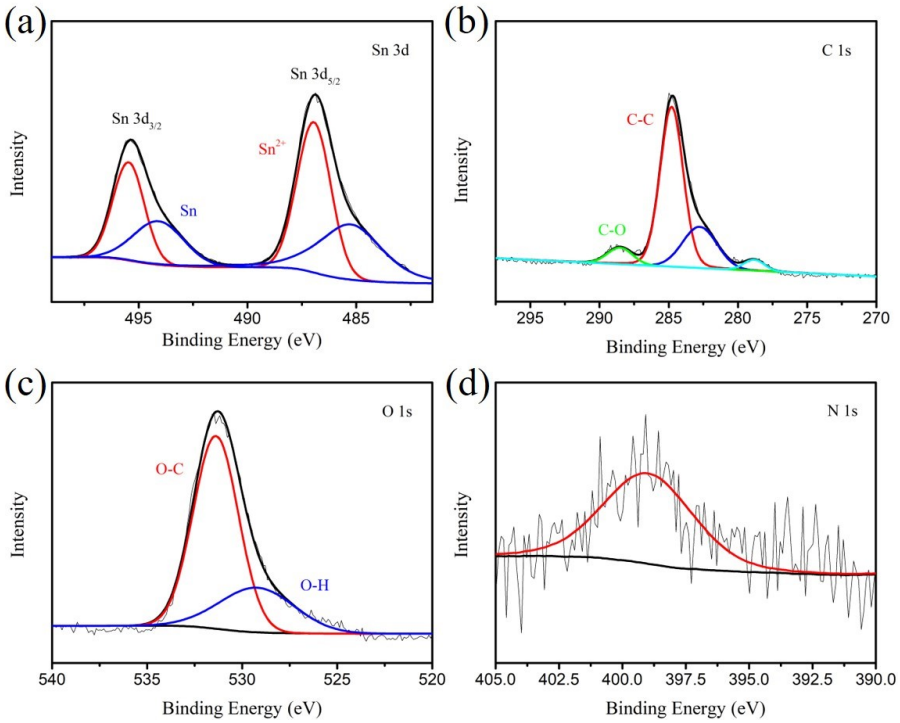

Figure S14. (a) High-resolution Sn 3d XPS spectrum. (b) High-resolution C 1s XPS spectrum. (c) High-resolution O 1s XPS spectrum. (d) High-resolution N 1s XPS spectrum.

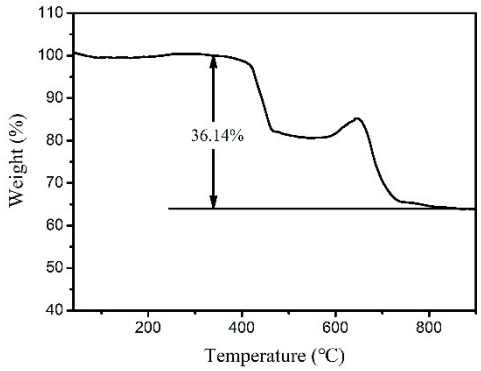

Figure S15. TGA of SnSe-C composite.

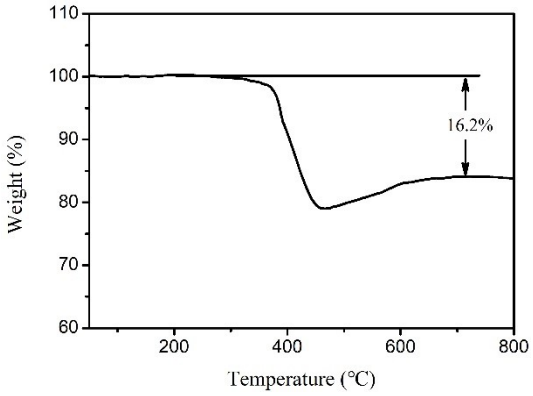

Figure S16. TGA of Sn-C composite.

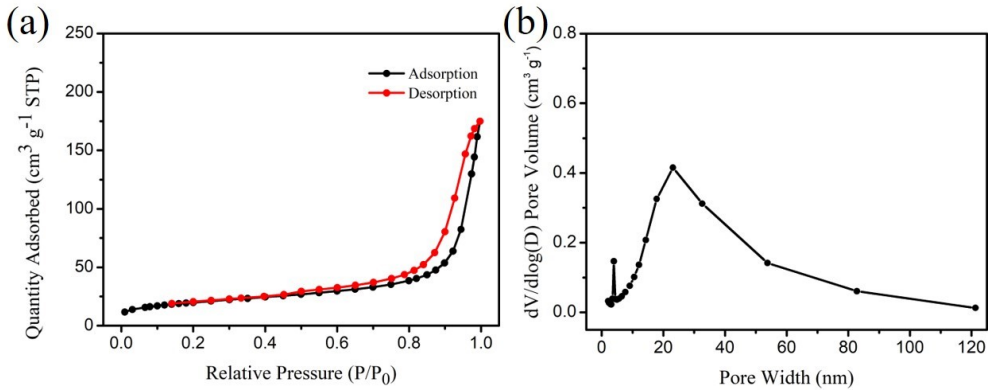

Figure S17. Specific surface area measurement of SnSe-C composite: (a) Nitrogen adsorption/desorption curve (b) corresponding pore size distribution.

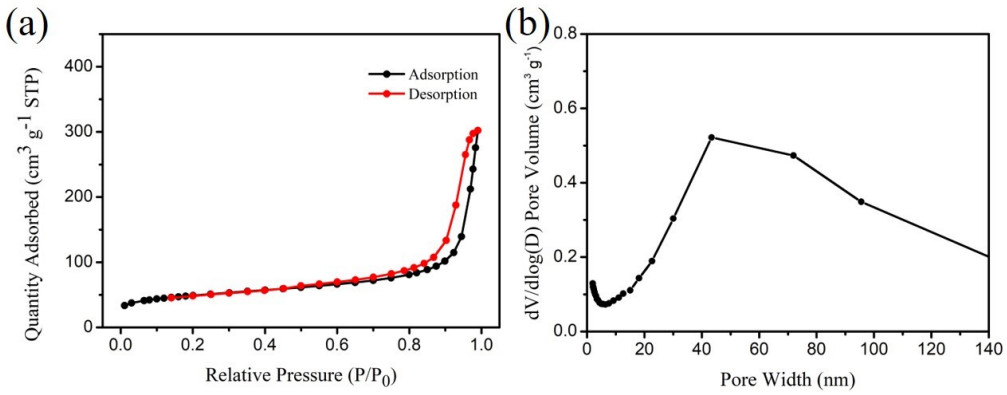

Figure S18. Specific surface area measurement of Sn-C composite: (a) Nitrogen adsorption/desorption curve (b) corresponding pore size distribution.

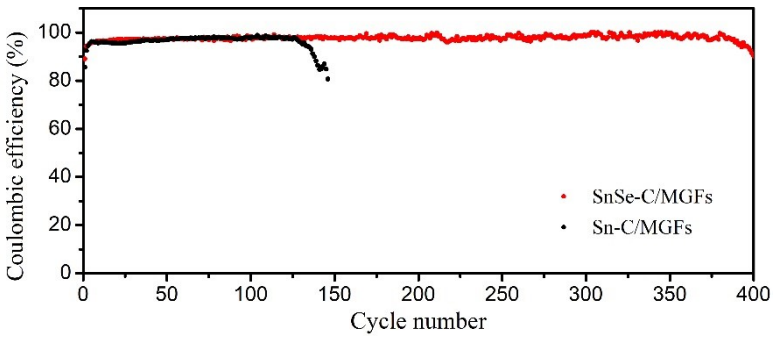

Figure S19. Coulombic efficiency of lithium plating on SnSe-C/MGFs and Sn-C/MGFs with amount of 1 mA h cm^{-2} at 2 mA cm^{-2}.

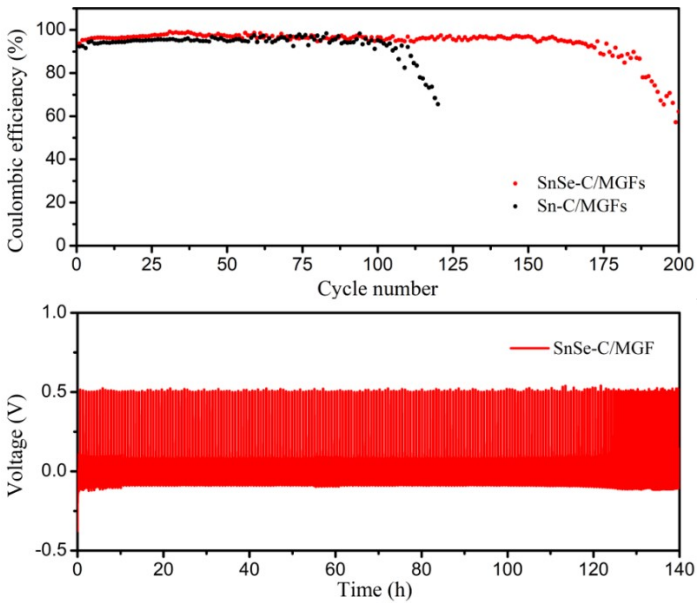

Figure S20. Coulombic efficiency of lithium plating on SnSe-C/MGFs and Sn-C/MGFs and corresponding discharge/charge curves with amount of 1 mA h cm^{-2} at 3 mA cm^{-2}.

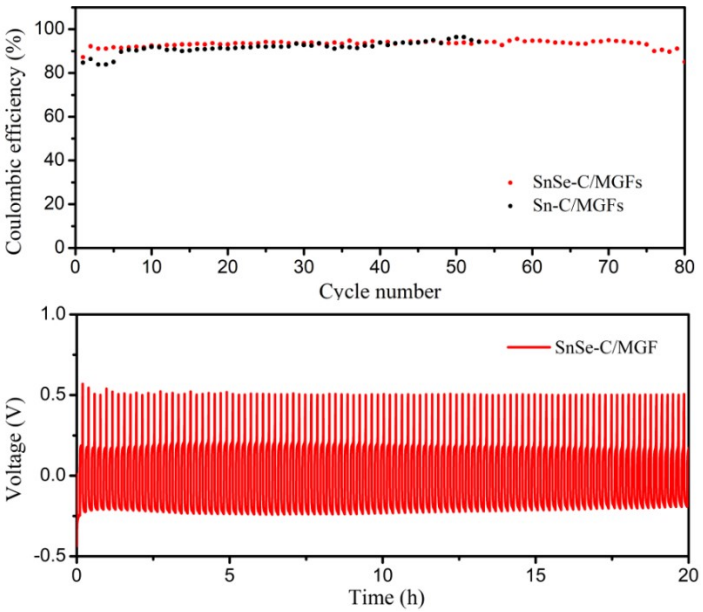

Figure S21. Coulombic efficiency of lithium plating on SnSe-C/MGFs and Sn-C/MGFs and corresponding discharge/charge curves with amount of 1 mA h cm^{-2} at 10 mA cm^{-2}.

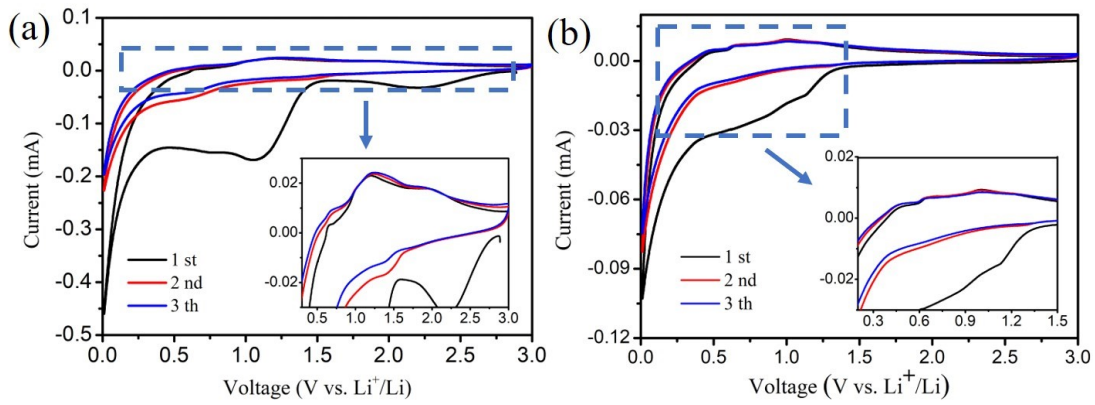

Figure S22. CV curves of SnSe-C/MGFs and Sn-C/MGFs anode countering to lithium metal plate. Test voltage range is from 2.0 V to 0.01 V and the sweep speed is 0.1 mV s^{-1}. (a) SnSe-C/MGFs; (b) Partial enlarged view of (a); (c) Sn-C/MGFs; (d) Partial enlarged view of (c).

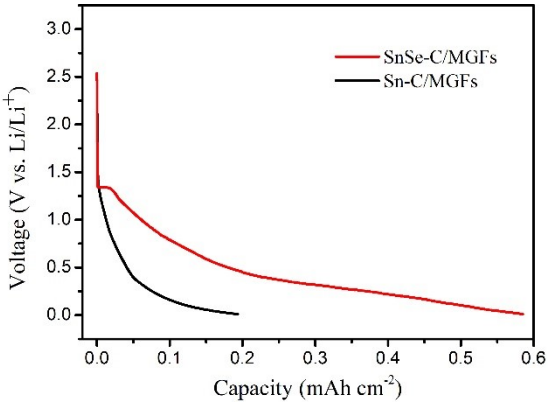

Figure S23. First cycle discharge voltage–time curve of SnSe-C/MGFs and Sn-C/MGFs at 0.05 mA cm^{-2}.

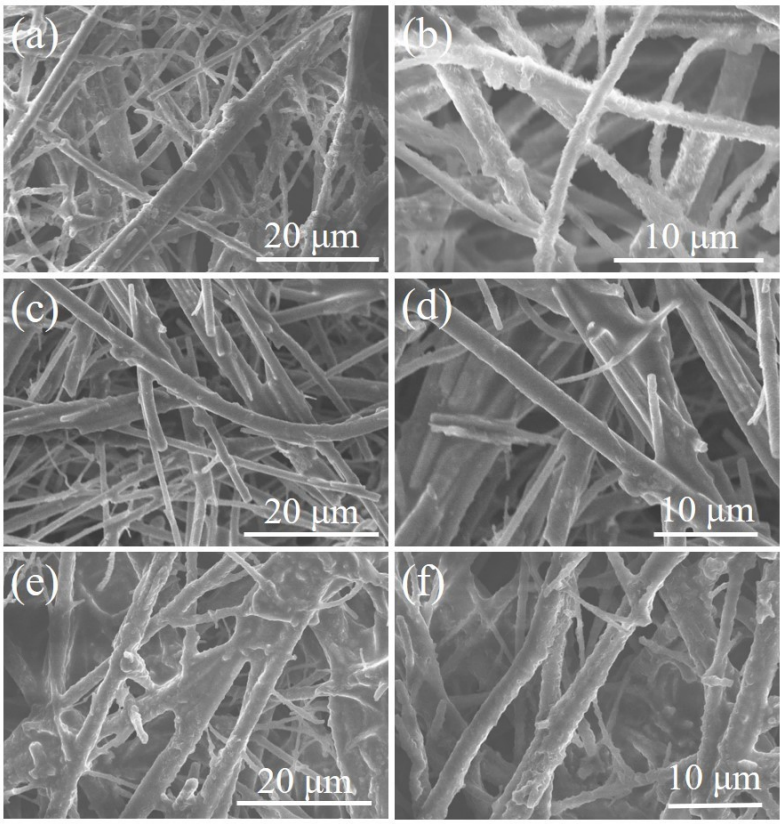

Figure S24. SEM images of the morphologies of lithium deposited on SnSe-C/MGFs at a current density of 1mA cm^{-2} with the capacity of (a-b) 1 mAh cm^{-2} (c-d) 3 mAh cm^{-2} (e-f) 5 mAh cm^{-2}.

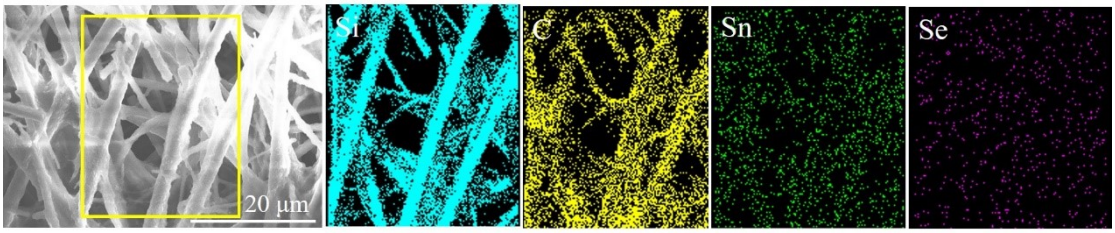

Figure S25. EDS elemental mapping diagram of Si, C, Sn and Se of the SnSe-C/MGFs after deposited 5 mAh cm^{-2} lithium.

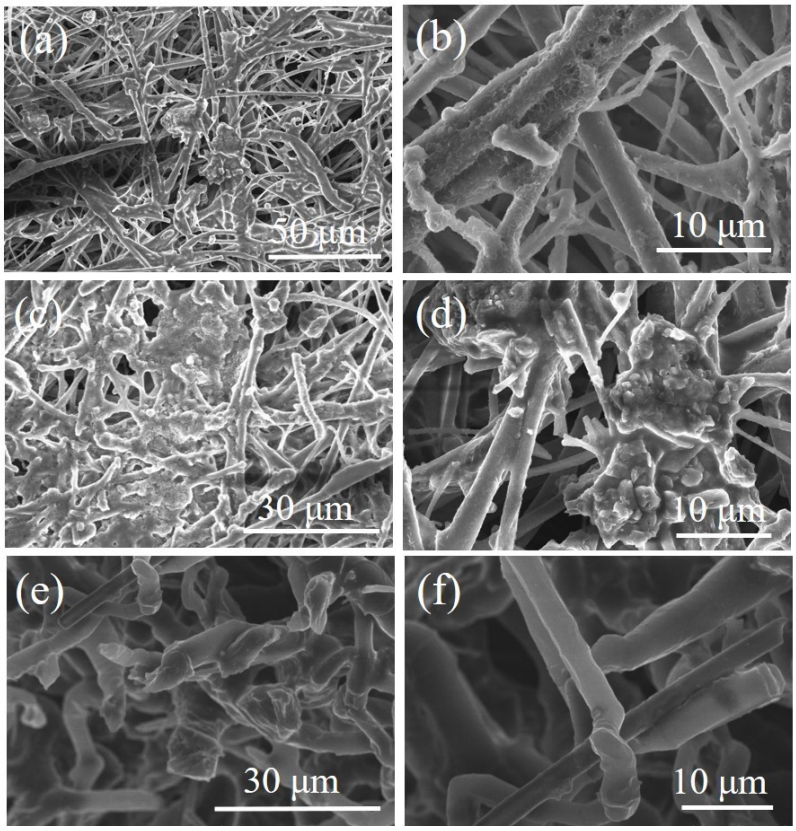

Figure S26. SEM images of the morphologies of lithium deposited on Sn-C/MGFs at a current density of 1mA cm^{-2} with the capacity of (a-b) 1 mAh cm^{-2} (c-d) 3 mAh cm^{-2} (e-f) 5 mAh cm^{-2}.

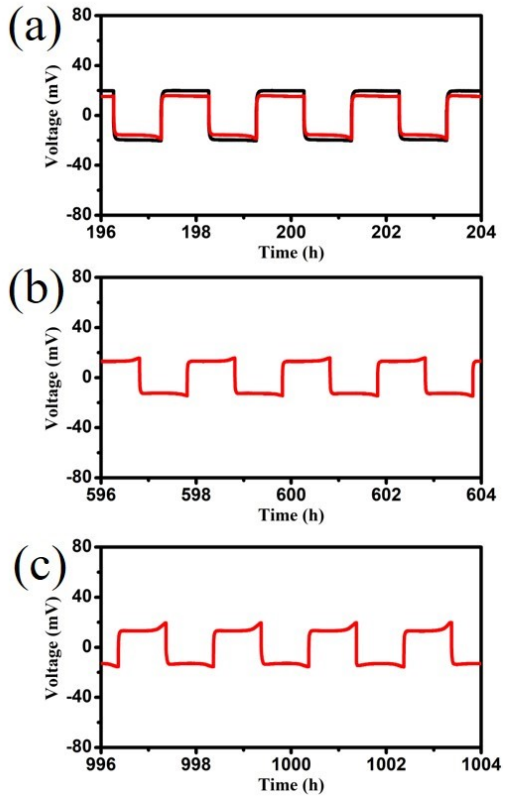

Figure S27. Partial enlarged voltage-time profiles of Figure 3a at 100th, 300th and 500th cycles.

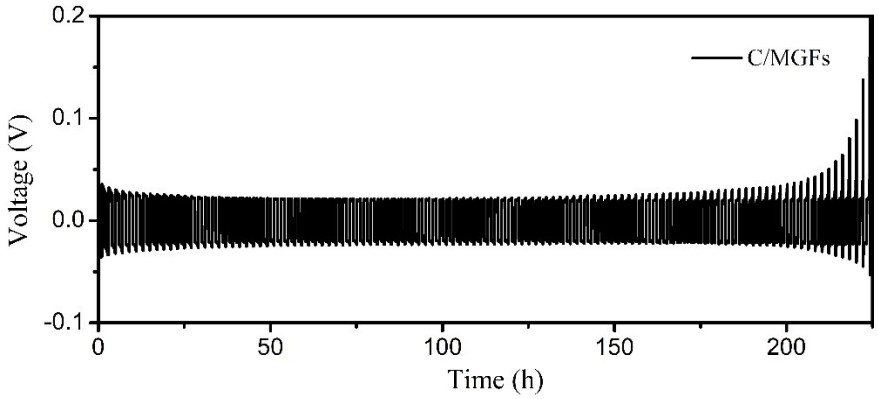

Figure S28. Voltage-time profiles of the symmetrical Li|Li/-C batteries with a capacity of 1 mA h cm^{-2} Li at 1 mA cm^{-2}.

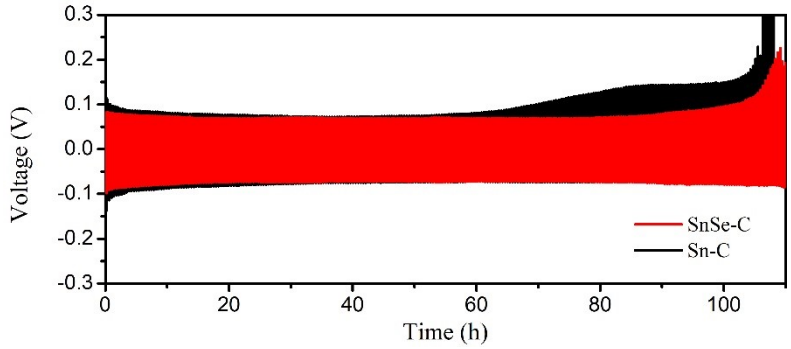

Figure S29. Voltage-time profiles of the symmetrical Li|Li/SnSe-C and Li|Li/Sn-C batteries with a capacity of 1 mA h cm^{-2} Li at 5 mA cm^{-2}.

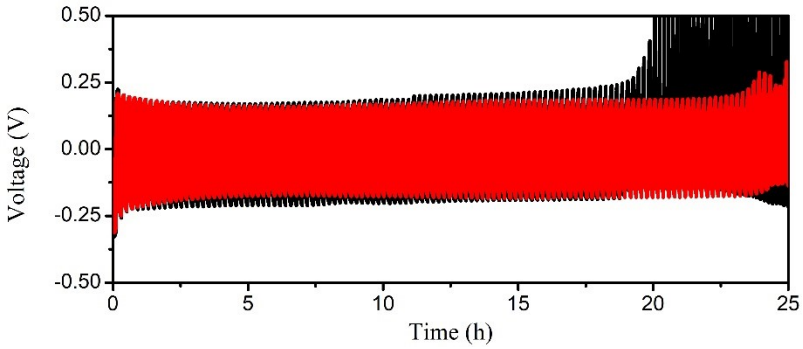

Figure S30. Voltage-time profiles of the symmetrical Li|Li/SnSe-C and Li|Li/Sn-C batteries with a capacity of 1 mA h cm^{-2} Li at 10 mA cm^{-2}.

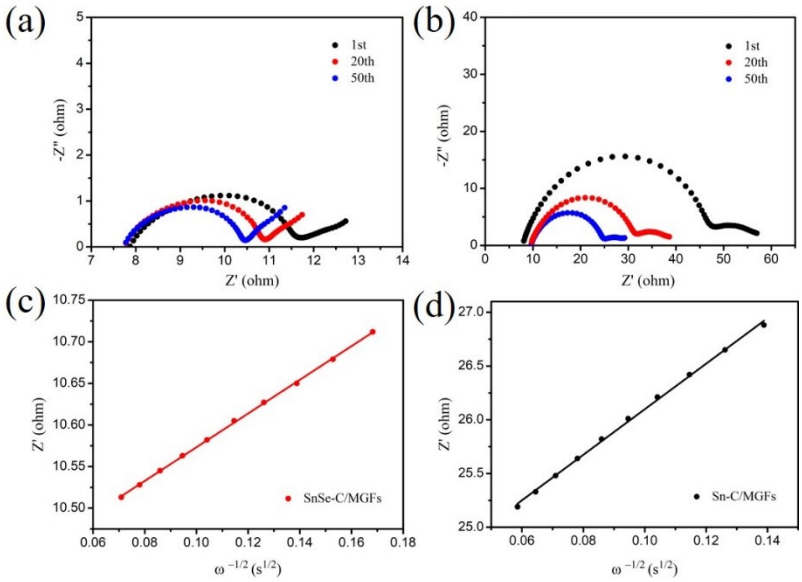

Figure S31. EIS curves of (a) Li/SnSe-C and (b) Li/Sn-C at different cycles in symmetrical cells. The fitted lines of the impedance versus $\omega^{-1/2}$ for Li/SnSe-C anode (c) and Li/Sn-C anode (d).

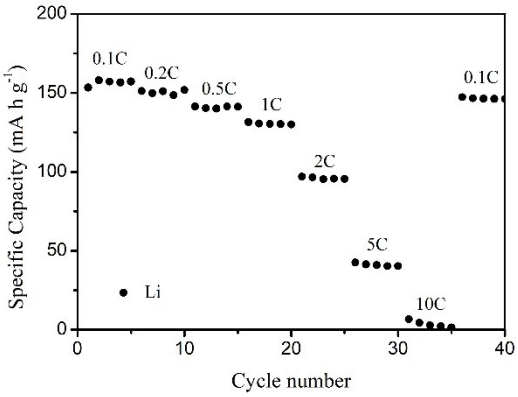

Figure S32. The rate performance of pristine Li in full cells.

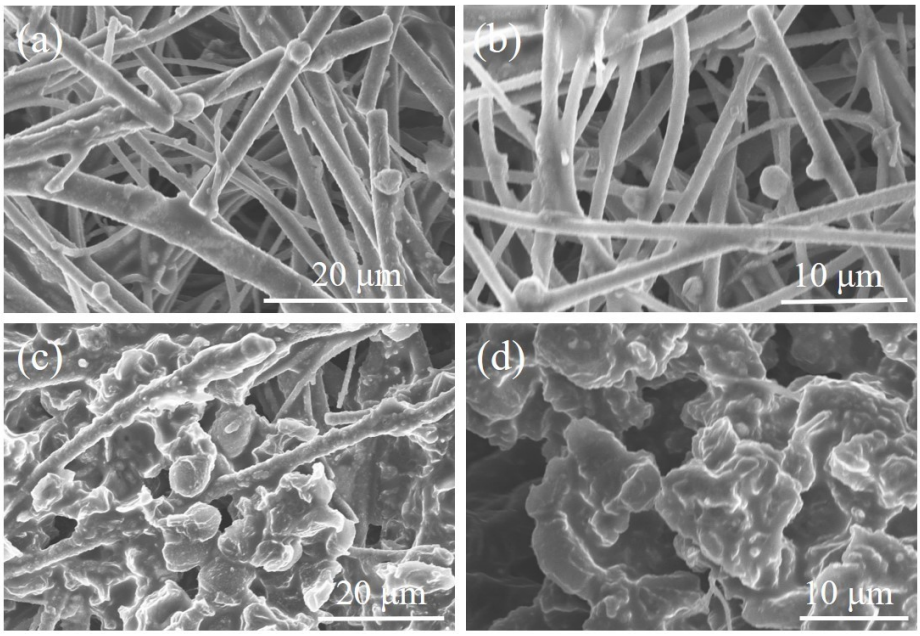

Figure S33. Morphologies of Li/SnSe-C anode (a-b) and Li/Sn-C anode (c-d) after 100 cycles at 2 C rate in full cells.

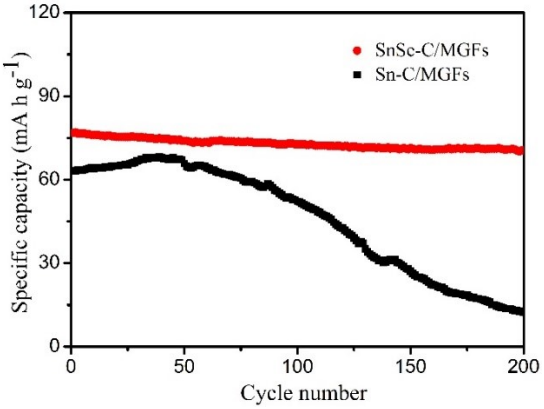

Figure S34. The cycling performances of Li/SnSe-C and Li/Sn-C at the rate of 5 C.

Table S1. Coulombic efficiency of SnSe-C/MGFs compared with various anode substrates.

substrates	Current/Capacity ($mA\ cm^{-2}$/$mAh\ cm^{-2}$)	CE (%)	cycle	Max current ($mA\ cm^{-2}$)	Ref.
PDA@3D Cu	0.5/1	97.3	200	1	*Energy Storage Materials*, 2020, 29, 84-91
ZnO@HPC	1/1	97.1	200	2	*Nano Energy,* 2017, 37, 177-186.
3D PI-coated copper	0.5/1	90	150	2	*Nat. Commun.* 2018, 9, 464.
g-C_3N_4@ Ni foam	2/1	97	140	3	*Adv. Energy Mater.* 2019, 9, 1803186.
Nitrogen-doped graphdiyne nanowall on Cu foam	1/1	98	250	5	*J. Mater. Chem. A*, 2019, 48, 27535-27546.
3D oxidized polyacrylonitrile nanofiber layer	3/1	71.3	120	3	*Nano letters,* 2015, 15, 2910-2916.
3D copper nanowire-phosphide	1/1	97.4	150	3	*Adv. Mater.* 2019, 31, 1904991.
This work	1/1	98.2	500	10	
	5/1	96.7	150		
	10/1	93.5	80		